Organic Chemistry Frontiers 8.4 (2021): 686-696

DOI: https://doi.org/10.1039/D0QO01110J

Exploring the Tubular Self-assembly Landscape of Dinucleobase Amphiphiles in Water

Paula B. Chamorro,[a] Fatima Aparicio,*[a] Raquel Chamorro,[a] Nerea Bilbao,[b] Santiago Casado,[c] and David González-Rodríguez*[a,d]

The design and production of the next generations of synthetic aqueous self-assembled systems able to mimic some biological features will require increasingly sophisticated monomer constituents that make use of additional interactions to hydrophibic effects to attain enhanced structural and functional complexity. Here, we broadly investigate the aqueous self-assembly of dinucleobase amphiphilic monomers into helical nanotubes under a wide range of different conditions of temperature, concentration, solvent composition and pH. Such monomers comprise an amphiphilic π-conjugated central block, endowed with a lipophilic chiral tail and a hydrophilic group that can be made anionic (carboxylate), neutral (glycol) or cationic (ammonium), disubstituted with complementary guanine and cytosine nucleobases at each termini. These molecules self-assemble into amphiphilic nanotubes in water but, when subjected to diverse (drastic) changes in the experimental conditions, undergo either disassembly into monomers, chiral reorganization, or a morphological restructuration into globular objects due to dehydration of the peripheral hydrophilic groups.

Introduction

Amphiphile self-assembly in aqueous media, a relevant process for healthcare, cosmetics or food technologies, is dominated by hydrophobic interactions. The H-bonded water network expels apolar moieties that are forced to interact together, whereas polar groups are efficiently solvated and exposed to the aqueous medium.[1-4] An apolar nano-environment is thus created, as classically illustrated in micelles or bilayers, into which other organic molecules can be incorporated.[5-8] These apolar nanospaces that are shielded from water are exploited by natural systems to profit from directional non-covalent interactions (like H-bonding, for instance) to achieve high selectivities and fidelities in molecular recognition and self-assembly processes, as seen in the active site of many enzymes or in DNA hybridization.

In the same way, aqueous synthetic assemblies are increasingly using more elaborate monomers in which such directional interactions are embedded in molecular structure, but shielded from water by strategically positioned lipophilic pockets.[9-19] This allows to attain higher levels of structural sophistication and, potentially, novel and complex functions in the designed self-assembled systems. Employing this strategy, we recently managed to confer a tubular shape to micelle assemblies by protecting directional Watson-Crick interactions between complementary nucleobases from the otherwise competing water medium.[20] Thus, in contrast to classical micelles of spherical shape, the presence of self-recognizing nucleobases in our monomer design allowed for an unprecedented supramolecular organization into cylindrical objects formed by stacked cyclic entities (Figure 1).

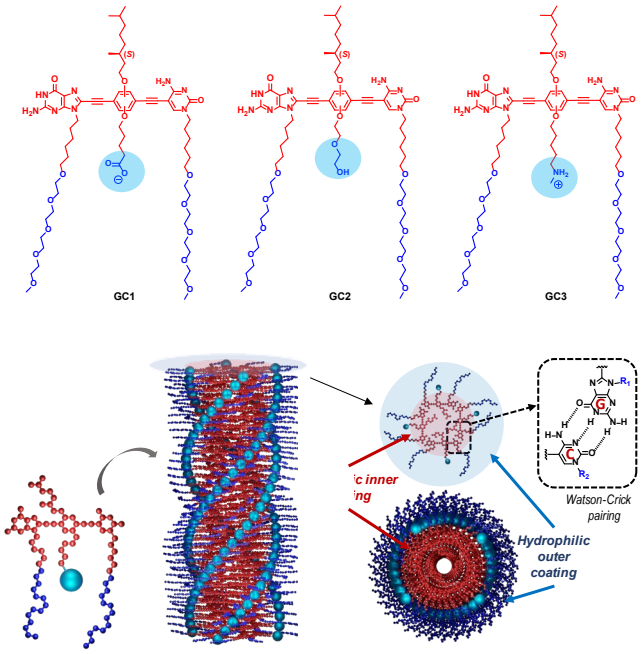

blue, respectively. (b) Scheme of the two-step self-assembly of GC monomers into nanotubes.

The general structure of our amphiphile monomers, as shown in Figure 1a, consists of a rigid π-conjugated central block disubstituted with complementary guanine (**G**) and cytosine (**C**) nucleobases in a linear fashion.[21-26] The central unit is made amphiphilic by installing a chiral lipophilic chain at one side and a hydrophilic tail at the other, which can be neutral or ionic. At the same time, the nucleobases are equipped at the *N*-1 or *N*-9

positions with a lateral chain comprising a hexamethylene apolar section followed by a tetraethyleneglycol residue. Upon Watson-Crick pairing,[27] an unstrained cyclic tetramer[28] can be formed in which this chain will always point to the exterior, so that the apolar inner segment serves to protect H-bonding from water whereas the outer glycol tail enhances water solubility.

In our previous work, we demonstrated that the nanotubes formed by **GC1** in water are constituted by this kind of H-bonded cyclic tetramer disks stacked on top of each other, likely driven by strong hydrophobic interactions between lipophilic sections and π-surfaces (Figure 1b).[20] The novel supramolecular tubular architecture generated presents a partially filled pore, of about 2 nm, that is primarily coated with lipophilic residues, as we demonstrated by encapsulating apolar dyes such as Nile Red. Such lipophilic coating is likely originated by the strong preference of the central block in adopting a conformation in which the lipophilic tails gather within the pore, while the polar (ionic) groups at the opposite side face the aqueous environment. Since the lipophilic chains are the ones bearing the chiral centre, it is supposed that the helical organization developed, as demonstrated by circular dichroism (CD) spectroscopy, originates from the interactions between these chiral groups within the tube pore. This was also proven by the proportional reduction in CD intensity as dye molecules are included into the pore, since they must hinder the communication between chiral centres.[20]

Thus, previous studies already suggested that the aqueous helical assembly of this kind of dinucleobase molecules is quite delicate and small changes in experimental conditions or in compound structure can affect substantially chiral organization. Here, we investigate further on this issue and broadly explore the self-assembly landscape of dinucleobase monomers **GC1**-**GC3** in water as a function of the three parameters that control self-assembly: temperature, concentration and environment, the latter meaning here solvent composition and pH. As shown in Figure 1a, **GC1**, **GC2** and **GC3** only differ in the hydrophilic pendant group at the central block: a carboxylic acid, a glycol or an amine, respectively, which can be made anionic (carboxylate), neutral or cationic (ammonium) within suitable pH ranges. Our results demonstrate that, although nanotube formation is highly reliable for all compounds in a wide set of experimental conditions, subtle changes in certain parameters or in compound structure can lead to nanotube dissociation, chiral reorganization, or even to a complete morphological modification of the aggregate.

Results and discussion

The complete characterization of compound **GC1** was recently published by our research group,[20] whereas novel dinucleobase monomers **GC2** and **GC3** were prepared following synthetic protocols (Scheme 1) that are briefly described here and further detailed in the S.I. of this paper.

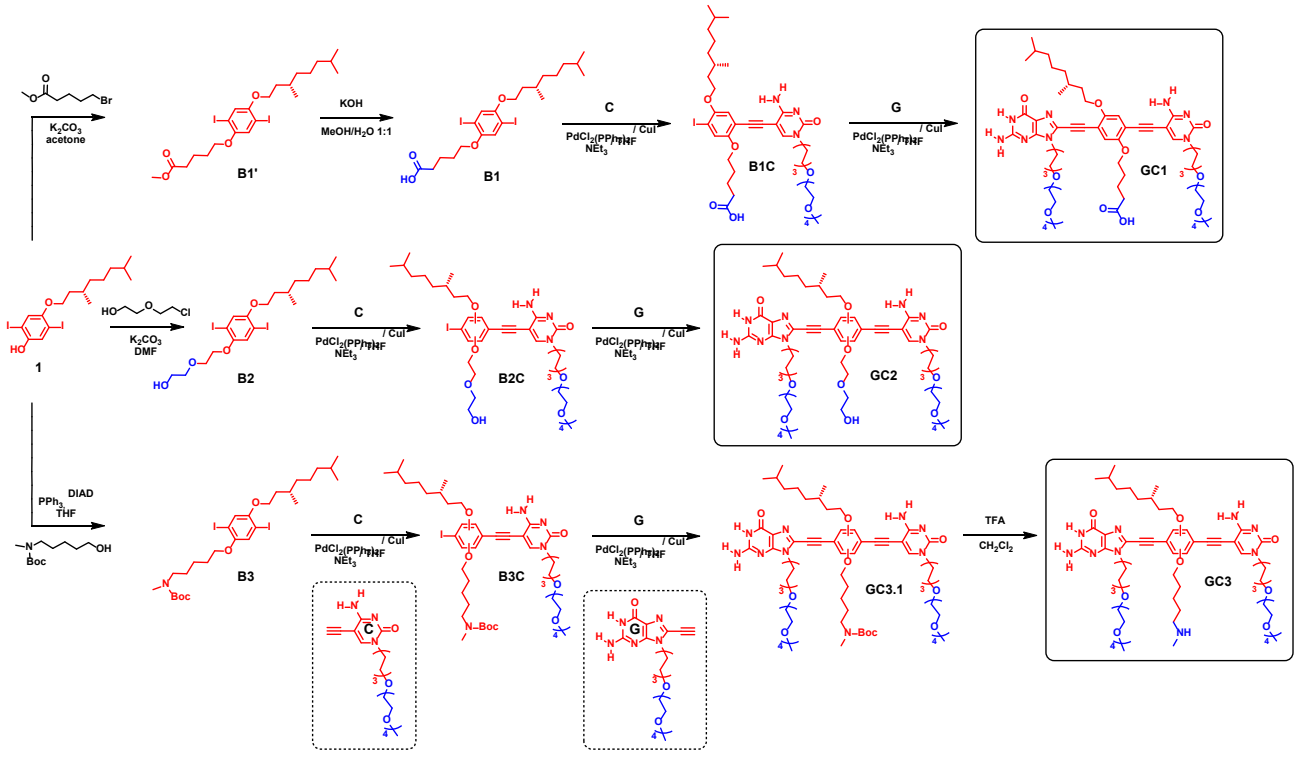

Scheme1 Synthesis of amphiphilic **GC1**-**GC3** dinucleobase derivatives.

The synthesis of these three monomers requires three main common fragments: the 5-ethynylcytosine **C**, the 8-ethynylguanine **G** and the diiodinated hydroquinone **1**, which is monoalkylated with the chiral chain derived from (*S*)-citronellol. The dihalogenated central blocks are generated from **1** by reaction of the unsubstituted OH group *via* Williamson or Mitsunobu-type protocols. This leads to compounds **B1'**, **B2** and **B3**, which are substituted with an ester, a glycol chain and a Boc-

protected amine, respectively. Ester **B1'** was then hydrolysed to the corresponding carboxylic acid **B1**. A first Sonogashira reaction with **C**, using a small excess of the central block to maximize the formation of the monosubstituted coupled product, yielded compounds **B1C**, **B2C** and **B3C**. These products are constituted by a mixture of regioisomers that are present in a (close to) 1:1 ratio, as determined by ^{1}H NMR, due to the low regioselectivity of the cross-coupling reaction. Their separation is quite challenging and reduces drastically the overall yield, so we decided to work directly with the mixture. The only exception is compound **B1C** for which, interestingly, this cross-coupling is fully regioselective and a single regioisomer was obtained. We believe the reason must be related to the stabilization of the corresponding isomeric organometallic Pd(II) complex by interaction between the C-amine and the carboxylic acid before reductive elimination. A solid proof that supports this hypothesis is that, when performing the reaction from ester **B1'**, a 1:1 mixture of regioisomers was again obtained. A second Pd-catalyzed coupling with the base **G** afforded dinucleobase monomers **GC1**, **GC2** and precursor **GC3.1**. Deprotection of the Boc group in the presence of TFA finally provided **GC3**.

The structural differences of **GC1**-**GC3** allows evaluating the influence of the chemical design in the formation of stable water-soluble supramolecular assemblies. Firstly, the water solubility of the dinucleobase derivatives was checked, being **GC1** and **GC3** soluble in this medium below moderate concentrations (> 10^{-3} M), whereas a small amount of THF was necessary to obtain clear solutions for compound **GC2**. The lower solubility of **GC2** in pure water was ascribed to the presence of a neutral residue at the central block instead of acid or basic substituents, which are able to (partially) ionize at suitable pH ranges. Thus, we assume that carboxylate groups in **GC1**, or ammonium groups in **GC3** are oriented to the outer part of the aggregate, contributing to the enhancement of their enhanced solubility in water.

A first indication of the self-assembly in solution of each compound was obtained by CD. In general, the presence of a CD signal for neutral water solutions of **GC1** and **GC3** and water-THF 9:1 solution of **GC2**, are indicative of the presence of aggregates with supramolecular chirality (Figure 2a). However, despite the structural similarity of these three molecules, their assemblies display quite different CD spectra in neutral aqueous media. These CD shifts parallel those observed in the absorption spectra of the three compounds, where they show a maximum around or below 400 nm, followed by a red-shifted shoulder at ~425 nm (Figure 2b). On the other hand, fluorescence emission intensity is quite low for all aggregates in water, in comparison to the monomer, while emission maxima, at 509 nm, is exactly the same for all systems (Figure 2c). Very similar features have been reported previously for the formation of supramolecular nanotubes from structurally related compounds in organic solvents.[20, 29]

Another important difference between the three monomers is related to the reliability of their helical organization. **GC1**, for instance, displays identical CD in a broad range of experimental conditions and we never observed kinetically trapped species (see below), meaning that the helical structure of these nanotubes is quite reproducible. Freshly dissolved **GC3**, on the contrary and as detailed below, showed soluble aggregated species with CD features that evolved with time to the thermodynamic assembly. However, for **GC2**, the corresponding CD signal changed in intensity and sign with time and/or sample preparation and no protocol could be found to obtain reproducible results. The actual helical structure of the **GC2** nanotubes is thus extremely sensitive to small changes in experimental conditions. This does not mean that the aggregate state or morphology changed, since absorption and, especially, emission spectroscopy consistently suggested the existence of aggregated species in solution (Figure 2b,c), while microscopy studies from aqueous samples always revealed elongated structures with the expected dimensions (Figures 2e and S1C-D). Since CD spectra was basically the only variable and uncontrollable feature for **GC2**, we attributed these effects to changes in the chiral chromophore arrangement influenced by a very subtle communication between chiral groups. Chiral order is induced by a single *S*-chiral stereogenic centre in the lipophilic chain at the central block. In addition to the different conformations that this chain can adopt, the central block can rotate so as to place the chiral group within or out of the pore and, furthermore, monomers **GC2** and **GC3** are actually composed of a 1:1 mixture of regioisomers (see S.I.) that have this lipophilic chain in *ortho*-position to either the C-ethynyl base or the G-ethynyl fragment. The reason why **GC1** and **GC3** do not show this variable behaviour is not clear, but tentatively attributed to the stronger hydrophilic character of the ionizable groups, which should make that a higher proportion of chiral lipophilic chains tend to group within the pore.

The morphology and size of the nanostructures formed in aqueous solution by these compounds could be studied on surface through atomic force and transmission electron microscopy (AFM and TEM, respectively; Figures 2d-f and S1A-F). The presence of nanotubular structures organized in aligned bundles with individual width dimensions between 5-6 nm in TEM and heights dimensions of 2-4 nm in AFM (Figure 2h), was confirmed. Considering our nanotube models and in agreement to our previous work,[20] the values found in TEM were in accordance with the expected outer diameter whilst the ones obtained by AFM resulted smaller, likely due to the compression

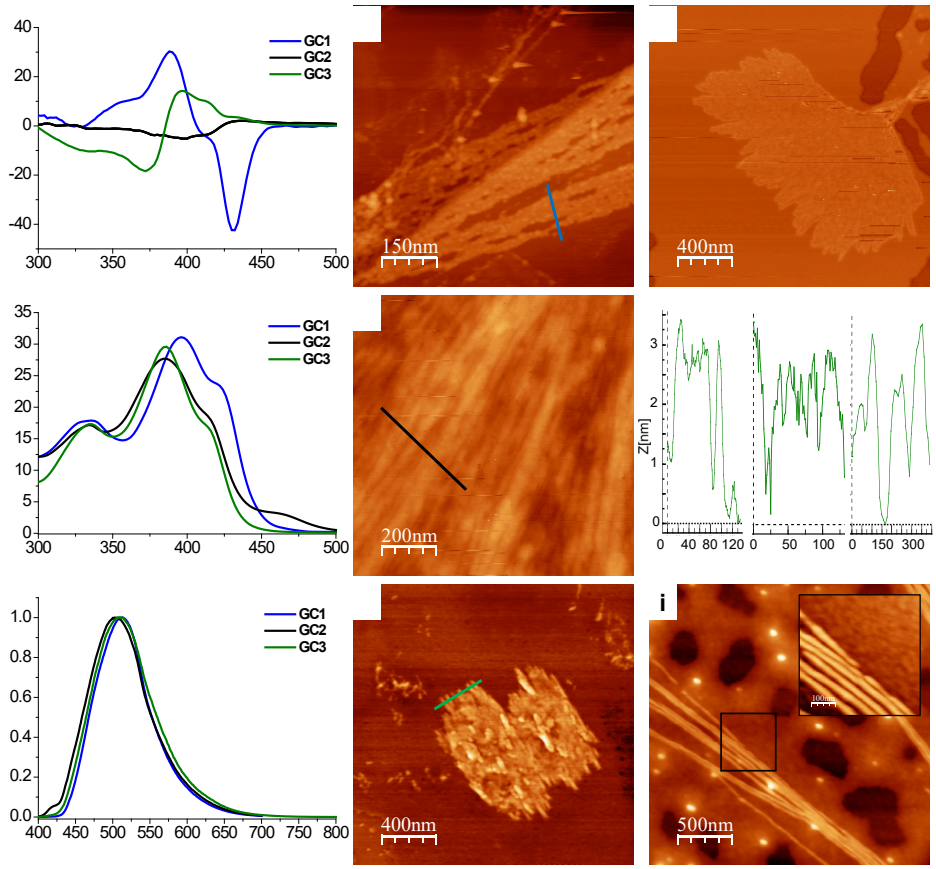

Fig. 2 Comparison of the spectroscopic features at $1.0 \cdot 10^{-4}$ M in water of **GC1** and **GC3** and in water/THF (9:1) of **GC2** by (a) CD, (b) UV-vis and (c) normalized emission at λ_{exc} = 380, 388 and 385 nm for **GC1**, **GC2** and **GC3**, respectively. (d,e,f) AFM images of **GC1**, **GC2** and **GC3**, respectively, drop-casted from aqueous solutions, and (h) corresponding height profiles along the blue, black and green lines in Figs. 2d-f. (g,i) AFM images in MeOH of the diluted gels of **GC1** and **GC3**, respectively.

of side-chains by the force applied by the AFM probe,[30] and by the affinity of the assemblies for the surface.

Next, with the aim to obtain more information about the tubular self-assembly of these dinucleobase derivatives and the range of experimental conditions in which they exist, or coexist with other aggregated species, a detailed supramolecular study was performed as a function of temperature, concentration, solvent composition and pH.

Effect of the Temperature

The supramolecular polymerization process of compounds **GC1**-**GC3** was studied in neutral aqueous solutions or in H_2O/THF mixtures by CD, UV-Vis and emission spectroscopy experiments as a function of the temperature (Figures 3 and S2A-S2L) within the 10^{-3}-10^{-6} M range. Two general conclusions extracted from these studies, as we detail below, are that: 1) the three compounds undergo almost identical cooperative polymerization processes, although their CD response, attributed to the aggregate helical organization, is not the same, and 2) the supramolecular behaviour at low concentrations (<10^{-5} M) is different than in the high concentration regime (>10^{-5} M).

At *low concentrations* (10^{-5} M or lower) a monomer-polymer transition is monitored as a function of temperature for all compounds. The non-sigmoidal absorption or emission cooling curves of **GC1**-**GC3** could be quantitatively analysed by a cooperative supramolecular polymerization equilibrium model (Figures 3a-c and S2A-C).[20] The corresponding fittings resulted in very similar thermodynamic values for all three monomers (Table 1), including: the elongation enthalpy (ΔH_e^0) and entropy (ΔS_e^0), the nucleation enthalpy (ΔH_n^0), the nucleation (K_n) and elongation (K_e) equilibrium constants, as well as their ratio: the cooperativity factor σ.[31] In this comparison it is important to remember that the analysis of **GC1** and **GC3** was performed in water, whereas for **GC2** a small amount of THF (10% v/v) needed to be added for solubility reasons. Still, the thermodynamic parameters of these three compounds do not differ importantly. In order to find identical conditions in which the three compound could be compared, we essayed the cooling curves at 10^{-5} M concentration with a volume fraction of THF (V_{THF}) of 0.1. However, in these conditions ionizable compounds **GC1** and **GC3** displayed very low degrees of aggregation that did not allow to record the polymerization process. When moving to higher concentrations, above 10^{-4} M, **GC2** was instead not soluble. We therefore fixed a solvent composition (V_{THF} = 0.2) and performed the temperature-dependent experiments at specific concentrations for each compound (higher for **GC1** and **GC3**, and lower for **GC2**) so that the polymerization process could be covered as much as

possible and fitted for the three compounds by the nucleation-elongation model (See Figures S2D-F and Table 1). A general trend found upon increasing the amount of THF is that the degrees of cooperativity tend to be lower, and become negligible for **GC2** at V_{THF} = 0.2.

Despite UV and emission trends were similar, the CD features and their evolution with temperature were very different for the three compounds at this 10^{-5} M concentration. As commented before, **GC2** aggregates displayed quite delicate and unreliable CD spectra, while the **GC3** nanotubes required very prolonged times (*i.e.* days; see below) to recover the original CD features after a heating cycle. For **GC1**, on the contrary, the polymerization process could be monitored as well by CD spectroscopy at $1.0 \cdot 10^{-5}$ M concentration in water. At high temperatures, the **GC1** CD signal is cancelled and then, below the elongation temperature (T_e), which coincides with the one registered in absorption and emission, it grows upon cooling. However, as shown in Figure S2A, the CD trends do not

Table 1 Thermodynamic Parameters Calculated for **GC1**-**GC3** upon Polymerization by Decreasing Temperature, and (b) Depolymerization by Increasing V_{THF}.

		K_n (M^{-1})[a]	K_e (M^{-1})[b]	σ [c/i]	ΔH^0 (KJ/mol)[d]	ΔS^0 (J/mol·K)[e]	ΔH_n^o (KJ/mol)[f]
GC1	**H_2O**	$4.1 \cdot 10^2$	$9.3 \cdot 10^5$	$4.4 \cdot 10^{-4}$	-40.6 ± 0.9	-21.9 ± 2.8	-19.2 ± 0.8
	H_2O/THF 8:2	$4.3 \cdot 10^2$	$2.0 \cdot 10^4$	$2.1 \cdot 10^{-2}$	-66.0 ± 1.7	-139.2 ± 5.5	-9.5 ± 0.4
GC2	**H_2O/THF** 9:1	$3.1 \cdot 10^2$	$4.0 \cdot 10^5$	$7.8\ 10^{-4}$	-40.6 ± 1.2	-28.8 ± 0.4	-17.7 ± 0.8
	H_2O/THF 8:2	$1.1 \cdot 10^4$		1.0	-123.8 ± 1.0	-33.8 ± 0.3	-
GC3	**H_2O**	$2.0 \cdot 10^2$	$5.4 \cdot 10^5$	$3.6 \cdot 10^{-4}$	-40.3 ± 2.6	-25.4 ± 0.8	-19.6 ± 2.3
	H_2O/THF 8:2	$8.3 \cdot 10^1$	$1.2 \cdot 10^5$	$6.8 \cdot 10^{-3}$	-36.3 ± 3.2	-4.3 ± 0.9	-12.4 ± 1.1

[a] Nucleation and [b] elongation constants, [c] degree of cooperativity, elongation [d] enthalpy and [e] entropy, and nucleation [f] enthalpy of the polymerization process calculated by decreasing T.

Table 2 Thermodynamic Parameters Calculated for **GC1**-**GC3** upon Depolymerization by Increasing V_{THF}.

	σ [a]	*m* (KJ/mol)[b]	ΔG (KJ/mol)[c]
GC1	0.56 ± 0.05	86.6 ± 4.9	-49.8 ± 1.6
GC2	0.49 ± 0.06	60.0 ± 1.6	-35.7 ± 0.2
GC3	0.58 ± 0.07	70.0 ± 1.8	-35.8 ± 0.3

[a] degree of cooperativity, [b] m Parameter and [c] Gibbs free energy of the depolymerization process observed by increasing V_{THF}.

overlap absorption and emission trends in the same conditions and also do not reach the expected plateau at low temperatures, but instead kept growing constantly with decreasing temperature. We attribute this effect to the fact that the self-assembled structures may keep increasing internal chiral order with temperature even after they are fully formed. We ruled out kinetic effects or the participation of intermediate species through several experiments that indicate that the samples are under thermodynamic equilibrium and that the CD effect depends only on sample temperature, but not on concentration or time. For instance, the comparison of cooling and heating curves of **GC1** (Figure S2G) discloses only very minor spectroscopic differences. In the same way, heating/cooling speed, from 0.2 ^oC/min to 5 ^oC/min, did not have a strong influence in the outcome of these experiments (Figure S2G). Finally, the samples left at low temperatures for prolonged time (*i.e.* several days) displayed the same CD intensities.

Now, *at high concentrations*, above 10^{-5} M, the supramolecular picture is quite different. At, for instance, $1.0 \cdot 10^{-4}$ M or higher concentrations, the CD signals of **GC1**-**GC3** did not disappear at high temperatures, but instead changed substantially, even in sign, which suggests important structural reorganizations of the aqueous aggregates (Figures 3d-f and S2H-K). Some changes in the UV-vis and emission spectra were also noted in these temperature-dependent experiments that were different from those observed in the low concentration regime and consistent with the fact that the dinucleobase compounds remain aggregated even at high temperatures. Again, some differences were found between the three compounds. For instance, while **GC1** exhibited a relatively fast transition between two CD-active states that can be monitored either along heating or cooling cycles at regular rates (1.0 ^oC/min; Figure S2H), **GC2** and **GC3** changed their CD spectra upon heating, but maintained it invariable along the cooling cycle experiment (Figures S2I-K). Only after a few days at low temperatures the original **GC3** CD signal was recovered (Figure S2L), indicating that the transition back to the thermodynamic state at room temperature is far slower for **GC2**/**GC3** than for **GC1**. For all compounds, these transformations could be reproduced for several cycles.

We believe this new helical aggregates originated at high temperatures result from the dehydration of the hydrophilic (ethylene oxide) chains above a critical temperature, similar to the case of lower critical solution temperature (LCST),[32-34] making these systems thermoresponsive at relatively high concentrations. Contrarily to classical LCST behaviour, we do not see any cloud point and the solubility of the solution remains unaltered, but we do detect drastic changes in the spectroscopic measurements, like the inversion of CD signal. In line with this, other authors have ascribed related spectroscopic changes to the interactions of supramolecular polymers with solvents.[35-37] Very recently, Aida´s research group reported a thermally bisignate supramolecular polymerization of a compound able to aggregate upon cooling, due to the clustering of the alcohol solvent employed, and also upon heating, because of the disruption of the dipole and hydrogen bonding interaction with alcohol.[35, 36] Both species presented spectral features that are well differentiated and did not overlap, which

allowed for an individual quantitative analysis. In contrast, the supramolecular structures found for **GC1** at low and high temperature display partially superposed spectroscopic properties which led to the appearance of different processes in the CD and emission trends that impeded their individual mechanistic analysis in these conditions. For **GC2**/**GC3**, in contrast and as commented above, the complete dehydration and hydration processes of the hydrophilic chains takes very long times, which again, impedes its quantitative analysis. Intrigued by this new aggregated species that is formed at high temperatures at relatively high concentrations, we performed AFM and TEM microscopy experiments on **GC1** and **GC3** samples deposited from warm (T > 80 ^{o}C) aqueous solutions. In addition to the typical aligned nanotube bundles that we always observe by these two techniques, the images now showed also higher ill-defined objects that are no longer longitudinal, but rather spherical in shape (Figures 3g and S2M-S2P). Thus, although structural details cannot be clearly extracted from these microscopy experiments due to the obvious experimental difficulties, it looks that, upon dehydration at high temperatures, the original **GC1**-**GC3** nanotube structure is transformed into another kind of globular aggregate.

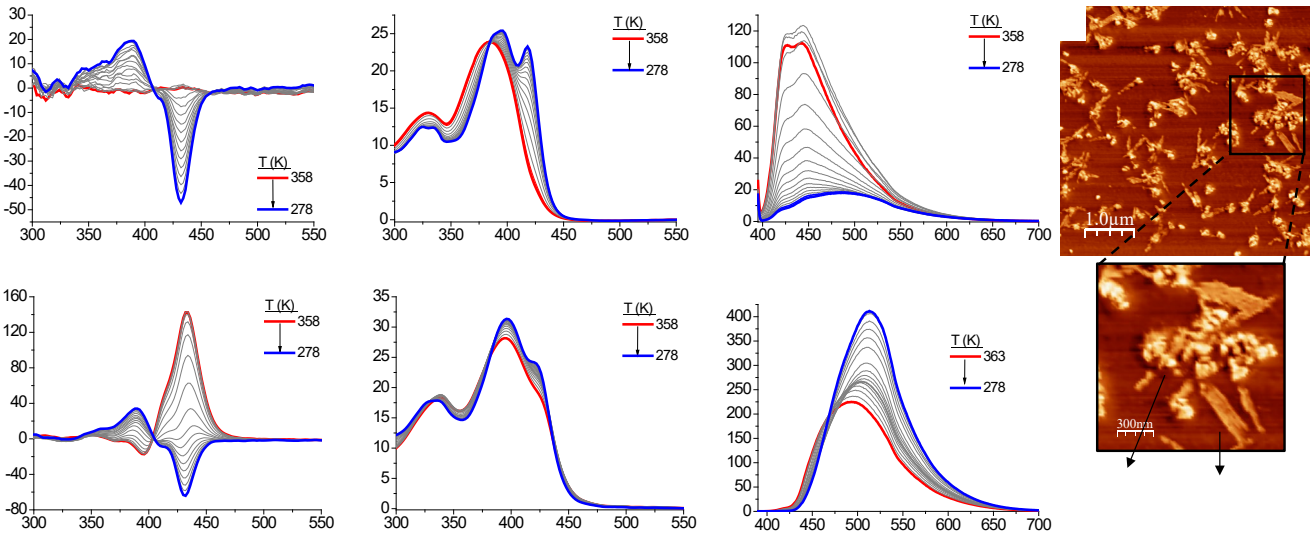

Fig. 3 Temperature-dependent CD (a,d), UV–vis (b,e), and emission (c,f) spectra of compound **GC1** in H_2O at $1{\cdot}10^{-5}$ M (top) and $1{\cdot}10^{-4}$ M (bottom). AFM images of the aggregates formed by compound **GC1** deposited from H_2O solutions at relatively high concentration ($5{\cdot}10^{-5}$ M) and high temperature onto HOPG.

Effect of the Solvent

We next studied these supramolecular systems through polymerization or depolymerization experiments at room temperature by changing the "good" (THF, MeOH or DMSO) and "bad" (H_2O) solvent composition.

Considering our previous background, THF was firstly selected as a denaturing solvent. Although THF alone is not a good solvent for **GC1**-**GC3**, since these molecules aggregate in pure THF (see below), they can be molecularly dissolved in a wide range of THF volume fractions (V_{THF}) in water, where the monomer spectroscopic features are detected. The most important spectroscopic changes that are recorded during the complete disassembly of the **GC1**-**GC3** supramolecular nanotubes upon increasing the volume fraction of THF in water are: 1) the disappearance of the CD signals, 2) the change in shape from a broader band in pure H_2O to a well-defined band with two maxima at *ca.* ~385-390 nm and ~410-415 nm, and 3) the increase in emission intensity and blue-shift of the emission maxima to below 500 nm (Figures 4 and S3A-S3C).

Attending to the emission spectra recorded (Figures 4c and 4g and S3A-S3C), which directly reports on molecular stacking, disaggregation is already noted at V_{THF} > 0.1 and it is complete in all cases at V_{THF} > 0.35 (see Figures 4d, 4h and S3A-S3C). This depolymerization emission trends could be fitted to the nucleation-elongation mechanism described by Meijer and coworkers[38] which allows to determine the Gibbs free energy gain upon monomer addition (ΔG^0), as well as the cooperative parameter (σ). Considering the quantitative thermodynamic analysis of **GC1**-**GC3**, it is important to note that all substances led to very similar degrees of cooperativity (σ = 0.58 for **GC1**, 0.49 for **GC2** and 0.56 for **GC3**) that are lower under these experimental conditions than in the previous temperature-dependent experiments (Table 1). The polymerization process was also recorded by emission spectroscopy for **GC1**, this time starting in the monomer state and decreasing V_{THF} gradually. As Figure S3D shows, polymerization and depolymerization transitions are virtually a superposition, which suggests that we are working in these experiments under thermodynamic equilibrium.

Now, when monitoring the same depolymerization transitions of **GC1** and **GC3** by absorption and CD spectroscopies (Figures 4d, 4h and S3A, S3C, S3D), which also report on relative molecular arrangements, more than one process is clearly differentiated (see Figure 4). During the depolymerization of **GC1**, up to V_{THF} ~ 0.1, CD intensity decreases and the signal evolves to another one that is only slightly different, while the

aggregate absorption band at 418 nm is slightly blue shifted (orange spectra in Figure 4). These spectroscopic features do not change significantly in the V_{THF} = 0.1–0.2 window, and then a second transition is recorded that leads to the disappearance of CD activity and the recovery of the monomer absorption features at V_{THF} > 0.3. The polymerization trends of **GC1** are very similar but not exactly overlapping, which we believe is due to the inherent experimental error in these experiments rather than to kinetic effects. Likewise, for **GC3**, as V_{THF} increases up to 0.1-0.2, the CD spectra evolves to a slightly different one which is also accompanied by absorption changes. Further increase in V_{THF} leads then to complete depolymerization.

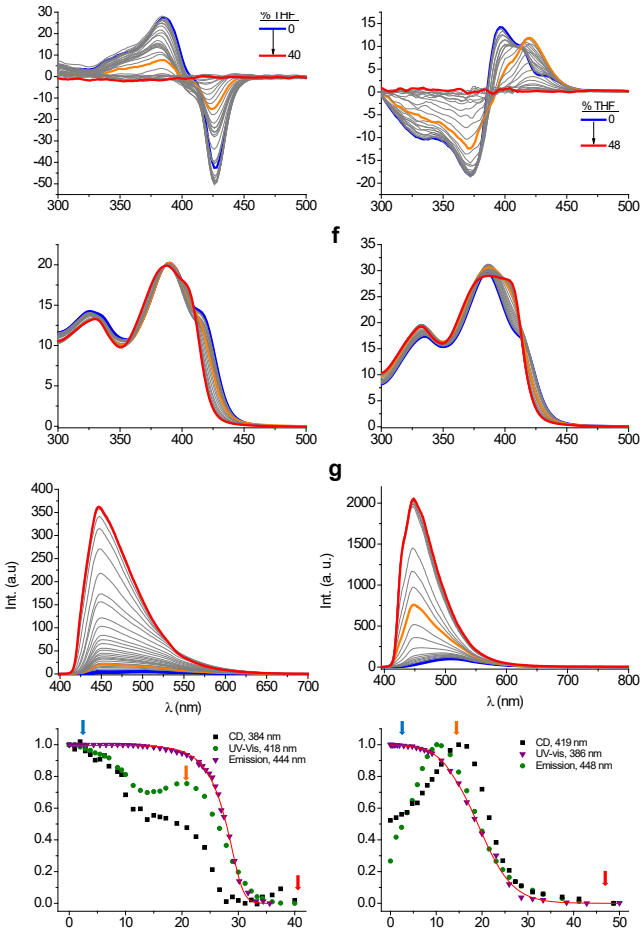

Fig. 4 CD (a, e), absorption (b, f), emission (c, g) spectral changes recorded as a function of solvent composition in H_2O-THF mixtures at 298 K of **GC1** (left) at $2.0 \cdot 10^{-4}$ M and **GC3** (right) at $1.0 \cdot 10^{-4}$ M. Spectroscopic trends recorded at specific wavelengths and fitting of the emission data to a solvent-dependent nucleation-elongation model (red line) for **GC1** (d) and **GC3** (h).

This overall picture seems to suggest that along the depolymerization/polymerization process other equilibrium intermediate aggregate(s) are being formed in which the molecular helical arrangement is only slightly different from the final self-assembled structure. This is actually not very surprising due to the amphiphilic nature of our supramolecular nanotubes. In addition to solvation changes that may occur at the tube exterior as V_{THF} is changed, the inner pore is only partially occupied by the lateral lipophilic substituents, so other (solvent) molecules must occupy the empty spaces. The change in solvent composition must have therefore some effect in the relative (chiral) arrangement between chromophores, and thus lead to slightly different equilibrium structures within different V_{THF} ranges.

In order to obtain a deeper insight into this depolymerization transitions as a function of solvent composition and to gather some structural evidence for the nature of the intermediate states detected by CD and absorption spectroscopies, ^{1}H NMR experiments at different H_2O:THF-D_8 compositions were made for **GC1**-**GC3** in exactly the same concentration range (Figures S3E and S3G). All compounds exhibit extremely broad proton signals in water that produce virtually flat ^{1}H NMR spectra, in agreement with the formation of large aggregates. On the other hand, at relatively large contents of THF, above V_{THF} = 0.4, the spectrum reveals sharp signals for each **GC1**-**GC3** proton, indicating that the monomers are molecularly dissolved, just like other spectroscopic techniques also point out. However, at intermediate V_{THF} values, aggregated species can be detected in slow exchange with the monomer in which the usual ^{1}H signals attributed to G:C pairing (H-bonded G-amide and C-amine protons at around 13.0 and 9.5 ppm) can be discerned in some cases (Figure S3E).

We discard that any of these intermediates consists in discrete cyclic tetramers, like in our previous work in apolar organic solvents,[29] since fluorescence intensity is significantly quenched below V_{THF} = 0.3, suggesting that π-π stacking interactions are still present within the intermediates structure. Our interpretation is that these are just growing nanotubes of oligomeric nature, since NMR signals are not yet too broad, and with slightly different spectroscopic features, due to slightly different relative molecular arrangements caused by solvation effects, than the final nanotubes generated in pure water. It is also important to mention here that none of the polymerization (cooling) or depolymerization (heating) transitions recorded as a function of temperature, even in H_2O/THF mixtures,[20] revealed the presence of intermediate structures, which suggests that their formation primarily depends on solvation changes.

Finally, and as anticipated above, **GC1**-**GC3** compounds aggregate again in 100% THF, a solvent that is able to solvate organic molecules more efficiently, but that does not compete as strongly for H-bonding as water. Whereas **GC1** and **GC3** produced insoluble aggregates in this solvent, **GC2** assemblies remained soluble and could be studied by spectroscopy and microscopy techniques. For instance, **GC2** aggregates in THF are CD-active and display broad, ill-defined ^{1}H NMR spectra, but disassemble upon increasing temperature or upon addition of a tiny amount of water (see Figure S3F and S3G). The morphology of the aggregates formed in THF solutions was also checked. The increase in the ratio of THF in H_2O/THF solutions led to the co-existence of circular objects of different sizes and tubular structures. When water was not present in solution, just circular objects were observed in the corresponding AFM and TEM microscopy images (Figures S3H and S3I). These results support the idea obtained from the previous analysis of the samples at high temperatures: when the nanotube samples are taken to

conditions that favour dehydration, they transform into a different kind of aggregate with globular shape.

We moved then to test a denaturing solvent of different nature, such as the protic solvent MeOH. A detailed inspection on the aggregation of these compounds in MeOH revealed that, just like THF, this solvent can be also used to disaggregate the nanotubular structures formed by, for instance, **GC1** and **GC3** in aqueous solutions (Figures S3J and S3K). In addition, while compound **GC2** was perfectly soluble in pure MeOH, dinucleobase compounds **GC1** and **GC3** revealed the presence of chiral aggregates by CD (Figures S3L and S3M). Unfortunately, their degree of polymerization was too low to study their self-assembly in detail, which resulted in low-intensity CD signals and the lack of significant changes in the absorption spectrum, even at the highest possible concentrations and at low temperatures.

Moreover, when the concentration of methanol solutions of compound **GC1** and **GC3** was increased further, the formation of gels with critical gelation concentrations around $1{\cdot}10^{-2}$ M (Figure S3P) was observed The characteristic fibrillary network of organogels was revealed by AFM, TEM and scanning electron microscopy (SEM), where a dense network of intertwined fibres, with dimensions that are in agreement with the expected nanotubes, was visualized (Figures S3N-S3R).

A third cosolvent was also considered for the investigation of the aggregation of compound **GC1** and **GC3**, this time the strongly polar aprotic DMSO. Once again, the increase of DMSO ratio in H_2O/DMSO mixtures provoked the disassembly of the **GC1**/**GC3** nanotubes obtained in water at $1.0{\cdot}10^{-5}$ M concentration (Figure S3S and S3T), just like when using THF or MeOH. However, for **GC1** we observed clear differences with respect these two solvents when recording the spectroscopic changes at higher concentration (>$\cdot 10^{-4}$ M). At this concentration, the increase in the ratio of DMSO from V_{DMSO} = 0.4 to 0.7 led to the appearance of a CD signal with opposite sense, that resembles the one detected at high temperatures and high concentrations in pure water (please compare Figures S3Sd-f and S2H). Once again, the change in solvent nature allowed us to reach the aggregates formed by the interaction of monomers with dehydrated hydrophilic chains. In order to obtain information about the morphology of these aggregates, microscopy experiments were performed to these intermediate H_2O/DMSO samples but, unfortunately, we only detected amorphous material. From V_{DMSO} = 0.8 to 1.0, this polar solvent, a strong competitor for H-bonding, is able to dissociate the **GC1** supramolecular structure and the CD activity is cancelled.

Effect of the pH

We finally evaluated the influence of the pH on the supramolecular polymerization of **GC1**, endowed with a carboxylate group, and **GC3**, which has a pendant ammonium group. Compound **GC2** was not considered in these studies because of its low solubility in pure water and the absence of relevant acid/basic sites. For **GC3**, surprisingly, no significant pH dependency was discerned, and this compound displays similar spectroscopic characteristics at 10^{-5} M or at 10^{-3} M concentration in a wide range of pH values, from pH = 3 to pH = 9 (Figure S4A and S4B). More basic pH values (pH > 12) resulted in no aggregation, presumably due to deprotonation of some of the relevant H-bonding sites in the nucleobases, like the G-amide proton. On the contrary, compound **GC1** presents different CD, UV-vis and emission spectra at acidic pH (pH = 3), compared to the ones observed at pH = 9 and pH = 5 (Figures 5 and S4A). More specifically, at pH = 3 aggregate emission is additionally quenched, the CD spectra develops into two maxima, and a decrease in absorbance was noted. It should be also mentioned that a precipitate was observed after keeping the sample at this acidic pH for some hours/days, which is in agreement with the notion that carboxylate groups are protonated and the solubility of the aggregates is reduced.

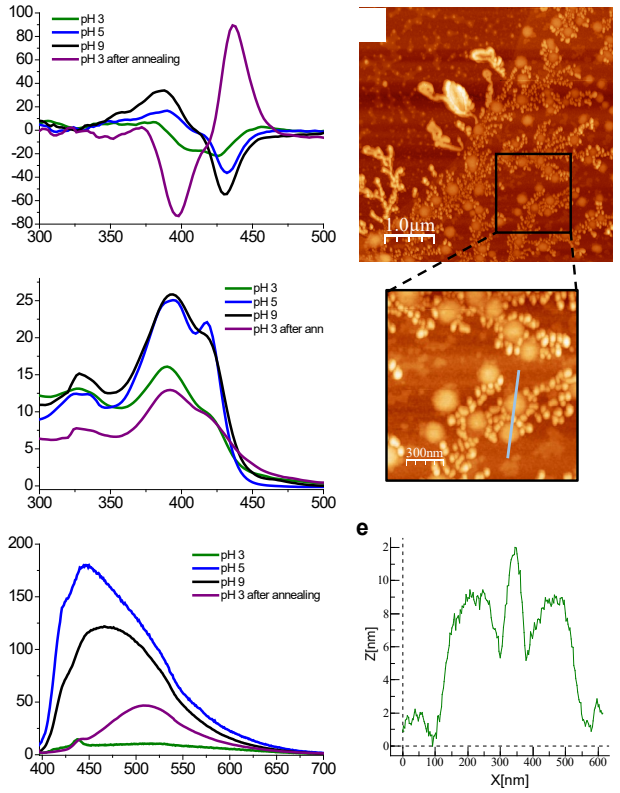

Fig. 5 Changes in the spectroscopic features of compound **GC1** as a function of the pH in water monitored by CD (a), UV-vis (b) and fluorescence (c) spectroscopies. (d) AFM images of the aggregates formed by the self-assembly of compound **GC1** at pH 3 ($1{\cdot}10^{-6}$ M) on mica. and (e) height profile along the grey line in (d).

We then compared the temperature-dependent behaviour of this **GC1** acidic sample (pH = 3) with the previously studied samples at neutral pH (pH = 5 or 7) or the samples at basic pH (pH = 9) at $1.0{\cdot}10^{-5}$ M. As exposed before, heating the neutral or basic solutions resulted in nanotube depolymerization (Figures S2A and S4C), showing identical spectral features and trends at both pH values. Interestingly, when the acidic sample was heated at 85 ^{o}C at this low concentration, the inverse CD signal was detected (Figures 5a and S4C), which resembles the one obtained at high temperatures and high concentrations, as described previously (Figure S2H). However, in contrast to the experiments carried out in neutral water (Figure S2A), the corresponding cooling experiment at pH = 3 (Figure S4C) didn´t allow reaching the original CD spectrum detected at room

temperature before annealing, and instead the CD sign observed at 85 ^{o}C was maintained along the whole experiment. This CD spectrum and supramolecular behaviour, strongly different from that observed at higher pH, suggests the formation of dehydrated aggregates of similar nature to the ones obtained at higher concentrations and neutral pH. The difference is that, upon cooling, the acidic samples do not recover the characteristic CD of the **GC1** supramolecular nanotubes, which is ascribed to the lower hydration capacity of the protonated carboxylic acids.

In order to fully characterize the supramolecular structures formed in acid media, microscopy studies were performed from **GC1** samples at pH = 3 and deposited over different substrates. The images obtained in both TEM and AFM microscopies showed again spherical objects with variable dimensions and heights ranging from 9 to 17 nm (Figures 5d, S4D and S4E), which clearly differ to the nanotubular structures formed by this compound at neutral or basic pH values, conditions in which the carboxylic acids are deprotonated.

Conclusions

In short, in this work we have swept across the aqueous self-assembly landscape of three amphiphilic G-C dinucleobase monomers that differ in the central pendant hydrophilic group (carboxylate, glycol or ammonium) by subjecting these molecules to drastic changes in temperature, concentration, solvent composition and pH. Depending on the experimental conditions, the nanotubular polymers consistently obtained in water underwent disassembly into monomers, chiral reorganization, or morphological restructuration into globular objects. The interpretation of our results, as exposed along the main text, allowed us to reach several main conclusions.

1) *The aqueous self-assembly of these three amphiphilic dinucleobase monomers into tubular structures with a cyclic tetramer section is quite reliable under a wide set of experimental conditions*. According to temperature- and solvent-dependent studies, all three molecules undergo very similar nucleation-elongation polymerization processes with related thermodynamic parameters and cooperativity factors. The nanotube products are sustained by a combination of noncovalent forces that are common and similar in magnitude for all three monomers. These include H-bonding between nucleobases, shielded from water by a lipophilic section, and, most importantly, hydrophobic interactions, that produce discotic cyclic tetramer sections with a lipophilic core and a hydrophilic perimeter (see Figure 1), which must generate strong stacking interactions along the tube axis. Nanotube diameters determined by microscopy and the G:C H-bonded proton signals detected in ^{1}H NMR experiments are key evidences that support such supramolecular structure.

2) *The chiral helicity, and thus the CD spectrum of the aggregated species is very sensitive to molecular structure and experimental conditions*, in particular to solvent composition. We believe this is due to the peculiar structure of our assemblies, where the lipophilic tails at the central block are expected to group within the nanotube pore, leaving the hydrophilic chain at the opposite side facing the aqueous environment. Since the chiral group is situated in these inner lipophilic tails, their interaction will govern inter-chromophore arrangement and, as a whole, the helical organization and relative chromophore arrangement within the nanotube. Hence, solvation changes can both affect the outer nanotube side and the partially filled nanotube pore by encapsulation of solvent molecules, which should have an effect on the organization of the chiral tails. As a result, along the polymerization/depolymerization transitions in mixtures of water and THF, we have detected the presence of intermediate aggregates with slightly different optical spectroscopic features. In addition, and this was very clear for **GC1**, the CD trends do not exactly follow the absorption and emission trends during cooling experiments under equilibrium conditions. This seems to reflect that the self-assembled structures may keep increasing internal chiral order with temperature even after they are fully formed, due to an increasingly optimal interaction between the inner chiral chains. Finally, it is interesting to note that the non-ionic **GC2** compound displayed multiple, often unreliable CD signatures as a function of the experimental conditions which, in line with our theory, could be due to a lower preference of the central block for conformations in which the chiral lipophilic tails are grouped within the pore, in comparison to the ionizable **GC1** and **GC3**, of a higher amphiphilic character

3) For a similar reason, and as expected, *ionizable carboxylate and ammonium groups in **GC1** and **GC3** led to tubular systems that displayed higher water solubility*, in comparison with the neutral hydroxy groups of **GC2**. In fact, **GC2** nanotubes required 10% of THF to be solubilized in an aqueous medium. Furthermore, such notable aqueous solubility was drastically reduced for **GC1** and **GC3** within pH ranges in which the ionic groups are protonated or deprotonated, respectively. In contrast, the solubility of **GC2** or the **GC2** aggregates was higher in organic solvents like THF or MeOH.

4) Finally, *a common feature of the three monomers involved the transformation of the supramolecular nanotube structure into other type of aggregates with globular morphology whenever a given experimental parameter was modified to a drastic extent that favoured dehydration of the nanotube peripheral hydrophilic groups*. This restructuration, quite typical of aqueous amphiphile assemblies with LCST behaviour, was found to occur at high temperatures above a given critical concentration, after addition of important amounts of an organic cosolvent, or at pH values that produced non-ionic species.

Conflicts of interest

There are no conflicts to declare.

Acknowledgements

Funding from the European Research Council (ERC-Starting Grant 279548 PROGRAM-NANO) and MINECO (CTQ2017-84727-P) is gratefully acknowledged. F.A. is grateful to MSCA-COFUND InterTalentum (713366) and MSCA-IF (793506)

programs. P.C. acknowledges the Comunidad de Madrid for the PEJ-2017-AI/IND-6246 contract.

Notes and references

1 M. R. Molla and S. Ghosh, Aqueous self-assembly of chromophore-conjugated amphiphiles, *Phys. Chem. Chem. Phys.*, 2014, **16**, 26672-26683.

2 A. Sorrenti, O. Illa and R. M. Ortuno, Amphiphiles in aqueous solution: well beyond a soap bubble, *Chem. Soc. Rev.*, 2013, **42**, 8200-8219.

3 B. Rybtchinski, in *Hierarchical Macromolecular Structures: 60 Years after the Staudinger Nobel Prize II*, ed. V. Percec, Springer International Publishing, Cham, 2013, DOI: 10.1007/12_2013_250, pp. 363-387.

4 A. Sikder and S. Ghosh, Hydrogen-bonding regulated assembly of molecular and macromolecular amphiphiles, *Materials Chemistry Frontiers*, 2019, **3**, 2602-2616.

5 C. M. A. Leenders, L. Albertazzi, T. Mes, M. M. E. Koenigs, A. R. A. Palmans and E. W. Meijer, Supramolecular polymerization in water harnessing both hydrophobic effects and hydrogen bond formation, *Chem. Commun.*, 2013, **49**, 1963-1965.

6 C. M. A. Leenders, M. B. Baker, I. A. B. Pijpers, R. P. M. Lafleur, L. Albertazzi, A. R. A. Palmans and E. W. Meijer, Supramolecular polymerisation in water; elucidating the role of hydrophobic and hydrogen-bond interactions, *Soft Matter*, 2016, **12**, 2887-2893.

7 N. M. Matsumoto, R. P. M. Lafleur, X. Lou, K.-C. Shih, S. P. W. Wijnands, C. Guibert, J. W. A. M. van Rosendaal, I. K. Voets, A. R. A. Palmans, Y. Lin and E. W. Meijer, Polymorphism in Benzene-1,3,5-tricarboxamide Supramolecular Assemblies in Water: A Subtle Trade-off between Structure and Dynamics, *J. Am. Chem. Soc.*, 2018, **140**, 13308-13316.

8 N. M. Casellas, S. Pujals, D. Bochicchio, G. M. Pavan, T. Torres, L. Albertazzi and M. Garcia-Iglesias, From isodesmic to highly cooperative: reverting the supramolecular polymerization mechanism in water by fine monomer design, *Chem. Commun.*, 2018, **54**, 4112-4115.

9 X. Lou, R. P. M. Lafleur, C. M. A. Leenders, S. M. C. Schoenmakers, N. M. Matsumoto, M. B. Baker, J. L. J. van Dongen, A. R. A. Palmans and E. W. Meijer, Dynamic diversity of synthetic supramolecular polymers in water as revealed by hydrogen/deuterium exchange, *Nat. Comm.*, 2017, **8**, 15420.

10 M. Ogasawara, X. Lin, H. Kurata, H. Ouchi, M. Yamauchi, T. Ohba, T. Kajitani, T. Fukushima, M. Numata, R. Nogami, B. Adhikari and S. Yagai, Water-induced self-assembly of an amphiphilic perylene bisimide dyad into vesicles, fibers, coils, and rings, *Materials Chemistry Frontiers*, 2018, **2**, 171-179.

11 P. P. N. Syamala, B. Soberats, D. Görl, S. Gekle and F. Würthner, Thermodynamic insights into the entropically driven self-assembly of amphiphilic dyes in water, *Chem. Sci.*, 2019, **10**, 9358-9366.

12 M. García-Iglesias, M. J. Mayoral, D. Serrano-Molina, F. Aparicio, V. Vázquez-González and D. González-Rodríguez, Self-Assembly of Diacetylene-Bridged Phenylenevinylene Oligomers in Water and Organic Solvents, *ChemPlusChem*, 2019, **84**, 488-492.

13 P. P. N. Syamala and F. Würthner, Modulation of the Self-Assembly of π-Amphiphiles in Water from Enthalpy- to Entropy-Driven by Enwrapping Substituents, *Chem. Eur. J.*, 2020, **26**, 8426-8434.

14 I. Helmers, B. Shen, K. K. Kartha, R. Q. Albuquerque, M. Lee and G. Fernández, Impact of Positional Isomerism on Pathway Complexity in Aqueous Media, *Angew. Chem., Int. Ed.*, 2020, **59**, 5675-5682.

15 M. R. Molla and S. Ghosh, Hydrogen-Bonding-Mediated Vesicular Assembly of Functionalized Naphthalene–Diimide-Based Bolaamphiphile and Guest-Induced Gelation in Water, *Chem. Eur. J.*, 2012, **18**, 9860-9869.

16 A. Sikder, D. Ray, V. K. Aswal and S. Ghosh, Stimuli-Responsive Directional Vesicular Assembly with Tunable Surface Functionality and Impact on Enzyme Inhibition, *Langmuir*, 2018, **34**, 868-875.

17 S. M. C. Schoenmakers, C. M. A. Leenders, R. P. M. Lafleur, X. Lou, E. W. Meijer, G. M. Pavan and A. R. A. Palmans, Impact of the water-compatible periphery on the dynamic and structural properties of benzene-1,3,5-tricarboxamide based amphiphiles, *Chem. Commun.*, 2018, **54**, 11128-11131.

18 A. Sikder, J. Sarkar, R. Barman and S. Ghosh, Directional Supramolecular Assembly of π-Amphiphiles with Tunable Surface Functionality and Impact on the Antimicrobial Activity, *J. Phys. Chem. B*, 2019, **123**, 7169-7177.

19 A. Sikder, D. Ray, V. K. Aswal and S. Ghosh, Hydrogen-Bonding-Regulated Supramolecular Nanostructures and Impact on Multivalent Binding, *Angew. Chem., Int. Ed.*, 2019, **58**, 1606-1611.

20 F. Aparicio, P. B. Chamorro, R. Chamorro, S. Casado and D. González-Rodríguez, Nanostructured Micelle Nanotubes Self-Assembled from Dinucleobase Monomers in Water, *Angew. Chem., Int. Ed.*, 2020, **59**, 17091-17096.

21 C. Montoro-García, J. Camacho-García, A. M. López-Pérez, N. Bilbao, S. Romero-Pérez, M. J. Mayoral and D. González-Rodríguez, High-Fidelity Noncovalent Synthesis of Hydrogen-Bonded Macrocyclic Assemblies, *Angew. Chem., Int. Ed.*, 2015, **54**, 6780-6784.

22 C. Montoro-García, J. Camacho-García, A. M. López-Pérez, M. J. Mayoral, N. Bilbao and D. González-Rodríguez, Role of the Symmetry of Multipoint Hydrogen Bonding on Chelate Cooperativity in Supramolecular Macrocyclization Processes, *Angew. Chem., Int. Ed.*, 2016, **55**, 223-227.

23 N. Bilbao, I. Destoop, S. De Feyter and D. González-Rodríguez, Two-Dimensional Nanoporous Networks Formed by Liquid-to-Solid Transfer of Hydrogen-Bonded Macrocycles Built from DNA Bases, *Angew. Chem., Int. Ed.*, 2016, **55**, 659-663.

24 C. Montoro-García, M. J. Mayoral, R. Chamorro and D. González-Rodríguez, How Large Can We Build a Cyclic Assembly? Impact of Ring Size on Chelate Cooperativity in Noncovalent Macrocyclizations, *Angew. Chem., Int. Ed.*, 2017, **56**, 15649-15653.

25 C. Montoro-García, N. Bilbao, I. M. Tsagri, F. Zaccaria, M. J. Mayoral, C. Fonseca Guerra and D. González-Rodríguez, Impact of Conformational Effects on the Ring–Chain Equilibrium of Hydrogen-Bonded Dinucleosides, *Chem. Eur. J.*, 2018, **24**, 11983-11991.

26 M. J. Mayoral, D. Serrano-Molina, J. Camacho-García, E. Magdalena-Estirado, M. Blanco-Lomas, E. Fadaei and D. González-Rodríguez, Understanding complex supramolecular landscapes: non-covalent macrocyclization equilibria examined by fluorescence resonance energy transfer, *Chem. Sci.*, 2018, **9**, 7809-7821.

27 M. J. Mayoral, C. Montoro-García and D. González-Rodríguez, in *Comprehensive Supramolecular Chemistry II*, Elsevier, Oxford, 2017, DOI: https://doi.org/10.1016/B978-0-12-409547-2.12536-3, pp. 191-257.

28 F. Aparicio, M. J. Mayoral, C. Montoro-García and D. González-Rodríguez, Guidelines for the assembly of hydrogen-bonded macrocycles, *Chem. Commun.*, 2019, **55**, 7277-7299.

29 V. Vázquez-González, M. J. Mayoral, R. Chamorro, M. M. R. M. Hendrix, I. K. Voets and D. González-Rodríguez, Noncovalent Synthesis of Self-Assembled Nanotubes through Decoupled Hierarchical Cooperative Processes, *J. Am. Chem. Soc.*, 2019, **141**, 16432-16438.

30 M. A. Beuwer, M. F. Knopper, L. Albertazzi, D. van der Zwaag, W. G. Ellenbroek, E. W. Meijer, M. W. J. Prins and P. Zijlstra, Mechanical properties of single supramolecular polymers from correlative AFM and fluorescence microscopy, *Polym. Chem.*, 2016, **7**, 7260-7268.

31 H. M. M. ten Eikelder, A. J. Markvoort, T. F. A. de Greef and P. A. J. Hilbers, An Equilibrium Model for Chiral Amplification in Supramolecular Polymers, *J. Phys. Chem. B*, 2012, **116**, 5291-5301.
32 S. Saeki, N. Kuwahara, M. Nakata and M. Kaneko, Upper and lower critical solution temperatures in poly (ethylene glycol) solutions, *Polymer*, 1976, **17**, 685-689.
33 M. Naya, K. Kokado, K. B. Landenberger, S. Kanaoka, S. Aoshima and K. Sada, Supramolecularly Designed Thermoresponsive Polymers in Different Polymer Backbones, *Macromol. Chem. Phys.*, 2020, **221**.
34 G. D. Smith and D. Bedrov, Roles of Enthalpy, Entropy, and Hydrogen Bonding in the Lower Critical Solution Temperature Behavior of Poly(ethylene oxide)/Water Solutions, *J. Phys. Chem. B*, 2003, **107**, 3095-3097.
35 K. Venkata Rao, D. Miyajima, A. Nihonyanagi and T. Aida, Thermally bisignate supramolecular polymerization, *Nat. Chem.*, 2017, **9**, 1133-1139.
36 K. V. Rao, M. F. J. Mabesoone, D. Miyajima, A. Nihonyanagi, E. W. Meijer and T. Aida, Distinct Pathways in "Thermally Bisignate Supramolecular Polymerization": Spectroscopic and Computational Studies, *J. Am. Chem. Soc.*, 2020, **142**, 598-605.
37 Y. Nagata, T. Nishikawa, M. Suginome, S. Sato, M. Sugiyama, L. Porcar, A. Martel, R. Inoue and N. Sato, Elucidating the Solvent Effect on the Switch of the Helicity of Poly(quinoxaline-2,3-diyl)s: A Conformational Analysis by Small-Angle Neutron Scattering, *J. Am. Chem. Soc.*, 2018, **140**, 2722-2726.
38 P. A. Korevaar, C. Schaefer, T. F. A. de Greef and E. W. Meijer, Controlling Chemical Self-Assembly by Solvent-Dependent Dynamics, *J. Am. Chem. Soc.*, 2012, **134**, 13482-13491.